Assessment and Projection of Water Budget over Western Canada using Convection Permitting WRF Simulations

Sopan Kurkute[1], Zhenhua Li[2], Yanping, Li[1,2], and Fei Huo[2]

[1]School of Environment and Sustainability, University of Saskatchewan, Saskatoon, SK Canada
[2]Global Institute for Water Security, University of Saskatchewan, Saskatoon, SK Canada

Correspondence: Zhenhua Li (zhenhua.li@usask.ca); Yanping Li (yanping.li@usask.ca)

Abstract. Water resources in cold regions in western Canada face severe risks posed by anthropogenic global warming as evapotranspiration increases and precipitation regimes shift. Although understanding the water cycle is key in addressing climate change issues, it is difficult to obtain high spatial and temporal resolution observations of hydroclimatic processes, especially in remote regions. Climate models are useful tools for dissecting and diagnosing these processes, especially, convection-permitting (CP) high-resolution regional climate simulation provides advantages over lower-resolution models by explicitly representing convection. In addition to better representing convective systems, higher spatial resolution also better represents topography and mountain meteorology, and highly heterogeneous geophysical features. However, there is little work with convection-permitting regional climate models conducted over western Canada. Focusing on the Mackenzie and Saskatchewan river basins, this study investigated the surface water budget and atmospheric moisture balance in historical and RCP8.5 projections using 4-km CP Weather Research and Forecast (WRF). We compared the high-resolution 4-km CP WRF and three common reanalysis datasets: NARR, JRA-55, and ERA-Interim. High-resolution WRF out-performs the reanalyses in balancing the surface water budget in both river basins with much lower residual terms. For the pseudo-global warming scenario at the end of the 21st century with RCP8.5 radiative forcing, both the Mackenzie and Saskatchewan river basins show increases in the amplitude for precipitation and evapotranspiration and a decrease in runoff. The Saskatchewan river basin shows a moderate increase of precipitation in the west and a small decrease in the east. Combined with a significant increase of evapotranspiration in a warmer climate, the Saskatchewan river basin would have a larger deficit of water resources than in the current climate based on the PGW simulation. The high-resolution simulation also shows the difference of atmospheric water vapour balance in the two river basins is due to flow orientation and topography differences at the western boundaries of the two basins. The sensitivity of water vapour balance to fine-scale topography and atmospheric processes shown in this study demonstrates that high-resolution dynamical downscaling is important for large-scale water balance and hydrological cycles.

1 Introduction

If the current pace of green-house gas (GHG) emissions continues, evidence points to fast-paced anthropogenic climate change in this century (Pachauri et al., 2014). The warming climate's impacts on water resources and ecosystems are generating considerable interest, particularly its impact on water balance in polar and subpolar regions. Most climate projections have

shown that polar and subpolar regions warm faster than the regions in lower latitudes (IPCC, 2013). These results have been robust both in projections of anthropogenic climate change and in observations due to the polar amplification from various local feedback mechanisms (Pithan and Mauritsen, 2014; Winton, 2006) and atmospheric heat transport (Hwang and Frierson, 2010). In the polar and subpolar regions of North America, the Canadian prairies and Canada's boreal forest will be strongly affected by climate change by the end of century.Climate change greatly affects water cycle, which closely couples with every aspect of ecosystem. Precipitation regime changes as moisture transport changes and storm tracks shift; evapotranspiration enhances as temperature rises; soil moisture decreases in summer due to larger evapotranspiration; snow amount increases in wetter winters and melts earlier as spring becomes warmer; river stream regimes change consequently. Due to these factors, how climate change will affect the water resources and water cycle is uncertain over the two largest river basins in western Canada,the Mackenzie and Saskatchewan river basins. It is important to enhance our understanding of the water budget in the two large river basins of western Canada.

Previous studies found it difficulty to close the water budget in observation in western Canada. Evapotranspiration and precipitation accounts for the exchange of water between the atmosphere and land. However, observing these processes on a large scale and at a high temporal resolution is costly and challenging. Remote sensing of evapotranspiration relies on thermal imagery and thus has difficulty estimating the temperature of land surface under cloudiness. The in-situ observations of evapotranspiration are only available to the locations of the flux towers. Both the observation and simulation of precipitation processes are challenging as a large range of scales from metres to thousands of kilometres involved. Observation of precipitation suffers from instrument bias and lack of coverage in the less populated regions.

Numerical models can enhance our understanding of the complex, nonlinear, interconnected hydro-meteorological processes in the Earth system by providing virtual laboratories. Through data assimilation and climate simulation, climate models can provide systematic overviews in investing aspects of water balance in land surface and atmosphere, which is difficult to comprehensively monitor through observation. However, the simulated changes in the water cycle from global climate models (GCMs) are of poor quality due to the relatively poor representation of the small-scale physical processes related to the water cycle, such as convection and orographic precipitation (Rasmussen et al., 2011). Climate simulations from GCMs have to be downscaled before their application in regional hydrology and ecology studies. The lack of explicit representation of small-scale processes also affects the quantification of the feedback of these processes to the large-scale atmospheric and hydrological processes. Therefore, dynamical downscaling using high-resolution regional climate models (Rasmussen et al., 2014) can more accurately represent various important hydroclimatic processes and provide projections without the assumption of stationarity.

Dynamical downscaling at convection-permitting resolution has advantage over coarser resolution due to their improvements in the simulation of convective precipitation (Prein et al., 2015) and more realistic representation of topography and lower boundary. Because convections contribute the most to extreme precipitations and the vertical transport of moisture, representing convective systems is critical in simulating precipitation and water balance. Convection-Permitting (CP) regional climate modeling can explicitly resolve deep convection and other local-scale hydroclimatic processes and their feedback on the larger scale systems. Moisture transport is significantly affected by the circulation response, which, in turn, is affected by the topog-

raphy through the generation of mountain waves and lee waves. For instance, Chinooks, the North American version of foehn, descend the lee of the Canadian Rockies, causing significant warming over the cold plains in winter. The concurrent warming at the surface and the heat transport by strong surface winds can have significant effects on water balance (MacDonald et al., 2018). For western Canada, particularly the Mackenzie and the Saskatchewan river basins, using high-resolution CP RCMs for hydroclimatic research is especially useful because of the large orographic features such as the Canadian Rockies and active convections during summer. We also want to compare the improvement of water balance closure in CP RCMs compared to several reanalyses and those in the paper by Szeto et al. (2008).

There have been several investigations utilizing coarse resolution datasets to study the water budget of the two basins. Szeto et al. (2008) used observation assimilated reanalysis datasets, including the National Centers for Environmental Prediction Global Reanalysis 2 (NCEP-R2), the global 40-yr European Centre for Medium-Range Weather Forecasts Re-Analysis (ERA-40), the NCEP North American Regional Reanalysis (NARR), and the Canadian Meteorological Centre (CMC) operational regional analysis as well as results from the Canadian Regional Climate Model (CRCM) simulations to investigate the water balance and energy balance in the Mackenzie River Basin (MRB). They found the residual terms in the water closure equation can be as large as budget terms in MRB, indicating the large uncertainties hydrological variables in the observation and the deficiencies in GCMs in regional-scale studies. Liu and Stewart (2003) used NCEP-NCAR reanalysis to calculate atmospheric moisture flux into and out of the Saskatchewan River basin and found its moisture flux characteristics is different from Mackenzie River basin, partly due to their topography and mean wind field. However, these studies are all based on relatively coarse resolution datasets, poorly representing convection and fine scale topography's effects on precipitation and moisture transport.

With the CP RCM simulation available over western Canada (Li et al., 2019), it is opportune to investigate several important questions regarding the water cycle in the two major river basins in western Canada:

1. How the water cycle and budget in CP RCM compared to reanalyses? we first compared the annual cycle of the components of surface water balance in the high-resolution model to several reanalyses to see whether the CP RCM closes the water balance better than reanalyses.

2. With better representation of the topography in CP RCM, how the fine scale topography can cause subtle differences in water balance and moisture flux between the two major river basins within the high-resolution RCM simulation.

3. Under a high-end emission warming scenario (RCP 8.5), how the water balance/cycle in the two river basins are going to change compared to the current climate.

This paper analyzes the impact of climate change on the water budget based on the CP RCM historical simulation (CTL) and RCP8.5 Pseudo Global Warming (PGW) simulation using the Weather Forecasting and Research (WRF) model. Section 2 describes the observation/reanalysis datasets and model configurations. Section 3 briefly describes the analysis and diagnostic methodology. Section 4 presents the comparison of water balance terms in WRF and reanalyses in detail and discuss it in the context of climate change and regional impacts. Section 5 discusses the results and section 6 summarizes the paper.

2 Numerical approach and data

2.1 Study domain and configuration of WRF

Two 15-year numerical experiments were conducted using Version 3.6.1 of WRF with a domain size of 639×699 grid points, a horizontal resolution of 4 km, and 37 vertical Eta levels with the model top at 50 hPa. The model domain covers parts of western

5   Canada (red frame in Fig. 1) from 46°-74°N latitude and 83°-150°W longitude. We used the New Thompson microphysics scheme (Thompson et al., 2008), the Yonsei University (YSU) scheme for planetary boundary layer (Hong et al., 2006). For short-wave and long-wave radiations, the Community Atmosphere Model (CAM) schemes from the CAM3 climate model were used (Collins et al., 2004). The land surface model component is Noah land surface model (Chen and Dudhia, 2001). With a 4-km horizontal resolution, the model explicitly resolves deep convection, and the deep cumulus parameterization was

10   turned off. No sub-grid cloud cover or shallow cumulus parameterizations were used, and spectral nudging was not applied. A more detailed description of the model setup can be found in (Li et al., 2019).
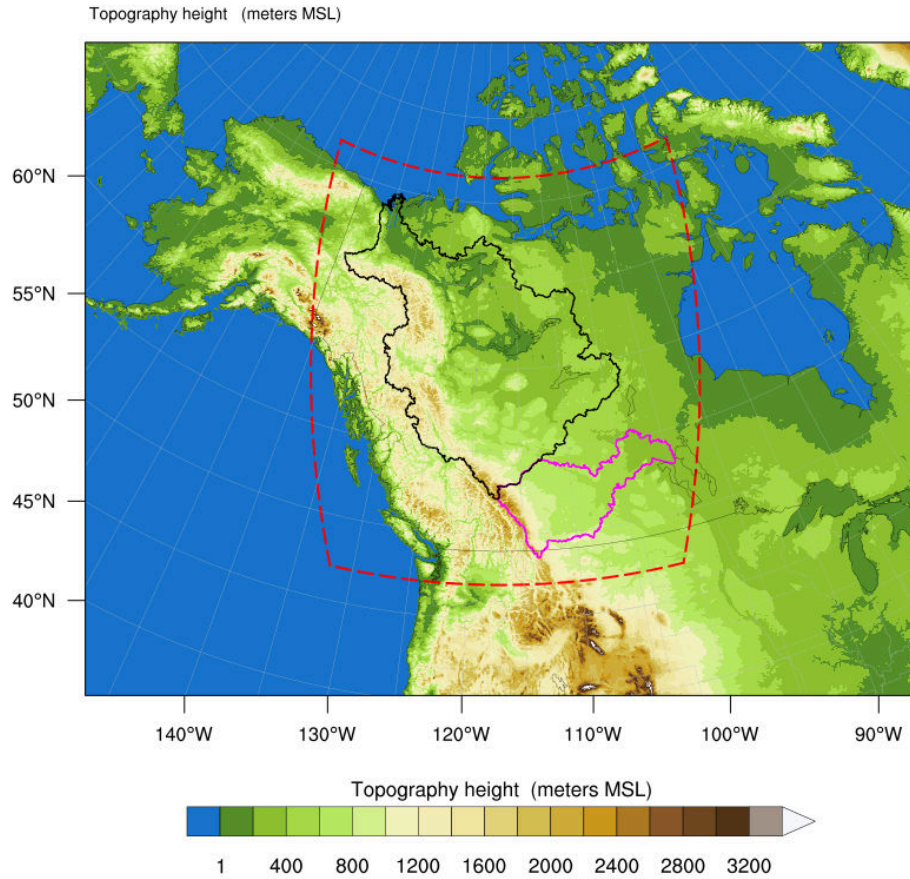
Figure 1. WRF simulation domain (2560 km × 2800 km) at 4-km grid spacing showing topographic height in meters above mean sea level (MSL). The simulation domain is indicated by a red frame. The bold pink and black polygons represent the MRB and the SRB.

2.2 Numerical experiments

Two 15-year experiments were conducted with historical and projected climate settings. The first experiment was a retrospective/control simulation intending to reproduce the statistics (variability and mean state) of the current climate within the domain. The current climate simulation extends from 1st October 2000 to 30th September 2015. This simulation was forced with 6-hourly the interim version of the next European Centre for Medium-Range Weather Forecasts Reanalysis (ERA-Interim(Dee et al., 2011)). Instead of using multiple reanalysis datasets, we only chose the best reanalysis data during the design phase of the project to force the WRF model due to the high computing cost of high resolution climate modeling at 4km. This retrospective simulation representing current climate is denoted as WRF-CTL.

For the pseudo-global warming simulation, denoted as WRF-PGW, is forced by the RCP8.5 scenario by the end of 21st century. We used a CMIP5 ensemble mean to deduce the climate change signal due to GHG forcing and conducted the simulation using a pseudo global warming approach. (Deser et al., 2012) argued that internal variability in individual simulations might cause large decadal differences even without the GHG-forced climate change. Besides, individual simulations cannot measure the range of climate sensitivity among GCMs. Therefore, an ensemble mean of 19 CMIP5 models was calculated to reduce the impacts of internal variability, model errors, and uncertainties in investigating the climate response to the GHG forcing under RCP8.5. These models were chosen based on their performances in simulating the late 21st century climate over North America. The perturbation was added to the initial fields in the sensitivity simulation following the PGW approach used in the work of Rasmussen et al. (2014, 2011). This 15-year (October 2000–September 2015) PGW simulation was forced with 6-h ERA-Interim reanalysis plus the climate perturbation:

$$WRF_{input} = ERA - Interim + \Delta CMIP5_{RCP8.5} \tag{1}$$

where $\Delta CMIP5_{RCP8.5}$ is the change of 95-year CMIP5 ensemble mean under the RCP8.5 emission scenario for all essential variables:

$$\Delta CMIP5_{RCP8.5} = CMIP5_{2071-2100} - CMIP5_{1975-2005} \tag{2}$$

The perturbed fields include all essential variables such as horizontal winds, geopotential height, temperature, specific humidity, sea surface temperature, soil temperature, sea level pressure, and sea ice.

The evaluation the WRF-CTL simulation was conducted in Li et al. (2019). The WRF-CTL simulation did a decent job in temperature and precipitation distribution compared to station data and gridded observation analysis.

2.3 Reanalysis Data

In this study, three different atmospheric reanalyses are used: NARR, ERA-Interim, and Japanese 55-year Reanalysis (JRA-55,Kobayashi et al. (2015)) as shown in Table 1.

2.3.1 (1) NARR

5   The NARR dataset from the National Centers for Environmental Prediction (NCEP) is used for diagnostic computation. Unlike other reanalysis in which precipitation is not assimilated, this reanalysis product assimilates high-quality and detailed precipitation observations as latent heating profiles (Mesinger et al., 2006). Though the methodology NARR employed to assimilate observation may introduce spurious grid scale precipitation (West et al., 2007), it is not a concern for our application that concerns mainly the monthly mean precipitation amount. The sparse availability of precipitation in the north also limits the

10   quality of NARR's precipitation over Canada compared to the US (Mesinger et al., 2006). The Noah land surface model included in NARR allows for more realistic land-atmosphere interactions than simpler land-surface schemes. The NARR data are available from October 1978 to November 2018 at a relatively high spatial (32 km horizontal) and temporal (3-h time interval) resolutions.

2.3.2 (2) JRA-55

15   JRA-55 is the latest long-term reanalysis data set produced by the Japan Meteorological Agency (JMA) operational data assimilation system (Ebita et al., 2011). This dataset features significant improvements over its predecessor, the Japanese 25-year Reanalysis with higher resolution, improved model physics, and an advanced data assimilation system with variational bias correction for satellite radiances (Ebita et al., 2011). JRA-55 is configured with horizontal spacing TL319 (about 55 km) and a hybrid sigma-pressure coordinate scheme using 60 levels up to 0.1 hPa, and provides vertically integrated meridional

20   and zonal moisture flux components. The land surface model of JRA-55 is Simple Biosphere Mode (SiB, Sellers et al. (1986, 1996)).

2.3.3 (3) ERA-Interim

ERA-Interim is produced by the European Center of Medium-range Weather Forecasts (ECMWF) with an improved atmospheric model and assimilation system that replaces that used in ECMWF Re-Analysis (ERA-40, Dee et al. (2011)). Additionally, the ERA-Interim dataset provides the vertically integrated divergence of moisture flux as data output, which can help us

25   diagnostically evaluate the results of the WRF model. This dataset is based on an atmospheric model and reanalysis system with 60 levels in the vertical with a top level at 0.1 hPa, and horizontal grid spacing with a T255 spherical harmonic representation (Dee et al., 2011). The land surface model of ERA-Interim is the Tiled ECMWF Scheme for Surface Exchanges over Land (TESSEL, Dee et al. (2011); Viterbo and Beljaars (1995); Viterbo et al. (1999)).

Table 1. Reanalysis products used in the comparison with WRF-CTL. P: precipitation, LH: latent heat,E: evaporation, QVAPOR, vapour mixing ratio.

Model name	Horizontal Resolution	Variables	Land Surface Model
WRF	4 km	U, V, QVAPOR, P, LH, Runoff	Noah
NARR	32 km	U, V, Specific Humidity, LH, P, Runoff	Noah
JRA-55	55 km	Vertically integrated moisture flux, P, Runoff, E	SiB
ERA-Interim	79 km	Vertically Integrated divergence of moisture flux, P, E, Runoff	TESSEL

2.4 Surface Water Budget

Water balance is an important constraint for understanding water availability and partition in model simulations and observations. The land surface components of water budget include precipitation (P), evapotranspiration (ET), runoff, and storage (snow water equivalent, soil moisture, canopy water, etc.). In the assessment of WRF simulation and reanalyses, there is no accounting for runoff transport between model grid points and horizontal movement of water. Thus, total runoff from WRF simulations represents the flux of water that is not taken up by or stored as soil moisture as in the study by Rasmussen et al. (2014). The surface water budget equation over the study regions can be written as

$$\frac{dS}{dt} = P - ET - Q + RESW \tag{3}$$

where $\frac{dS}{dt}$ is the change in the storage of water (S) in and above the ground over time, P is precipitation, ET is evapotranspiration, Q is runoff, and RESW is the residual. Equation (3) describes the partitioning of P into ET, runoff, and storage in land. The residual forcing is combined with the tendency term (i.e., $RESW = ET - P + Q + \frac{dS}{dt}$) in assessing the water balance closure. In this study, we estimated an annual budget of the surface water budget for MRB and SRB. The performance of the high-resolution WRF model was assessed by comparing the surface water budget with available reanalysis data products.

2.5 Atmospheric Moisture Budget

The atmospheric moisture budget provides an additional method for the evaluation of P - E in the RCM simulation. The spatially averaged water budget of atmosphere relates to the surface water budget in the following way:

$$\frac{dW}{dt} = E - P - \nabla \cdot MF \tag{4}$$

Here, E is the evapotranspiration, P is the precipitation, $\nabla \cdot$ is the horizontal divergence operator, W is the total columnar liquid content per unit area, and MF is the vertically integrated moisture flux $(kgm^{-1}s^{-1})$ given by

$$MF = -\frac{1}{g} \int_{psurf}^{ptop} qV dp \tag{5}$$

where q is the specific humidity in $kgkg^{-1}$, g is the gravitational acceleration constant of $9.8ms^{-2}$, dp is the change in pressure from land surface to the top of the atmospheric model (50hPa), and V is the horizontal wind vector given by

$$V = u\mathbf{i} + v\mathbf{j} \tag{6}$$

where u and v are wind components along east and north direction respectively. The horizontal divergence of the vertically integrated moisture flux $\nabla \cdot MF$ is the main variable of interest in this study. A negative value of moisture divergence corresponds to moisture convergence.

3 Results

3.1 Surface Water Budget

Figure 2 shows both the peak and annual runoffs in MRB in the WRF model are comparable to those in JRA-55 and much larger than the other reanalyses, which is partly related to their estimations in winter precipitation and storage terms such as
5 snow cover and soil moisture are larger (Li et al., 2019). Another factor is how the WRF model's Noah LAM models the frozen soil permeability. The Noah land surface model treats the frozen soil permeability as in Koren et al. (1999), which is shown to underestimate the infiltration of water through frozen soil and generate excessive surface runoff in spring over the Arctic river basins because the model's frozen soil permeability is too small (Niu and Yang, 2006). In cold regions, melting of snow accumulated over the winter generates high flows orders of magnitude larger than the winter discharge (Woo, 2008). Runoff
10 and the change of storage dominate in spring and peak in May in the WRF simulation and JRA-55 and reaches the maximum in summer in NARR. The spring peak runoffs in WRF and JRA-55 are about 3mm day^{-1}, three times as large as observation (Yang et al., 2015). The winter runoff in WRF and NARR is close to 0, whereas observation shows a 0.2 mm day^{-1} runoff in winter (Yang et al., 2015). Runoff is much smaller in NARR and ERA-Interim and significantly less than observation (Yang et al., 2015) in spring, summer and autumn due to their unrealistically small storage terms.

15 Figure 3 shows tha both the WRF simulation and the NARR reanalysis show a better balance between P, ET, the change of storage, and runoff in SRB, with the lowest residual term for all months. Both JRA-55 and WRF present a peak runoff in April, whereas ERA-Interim shows that runoff is negligible compared to other terms throughout the year. The residual term in JRA-55 is large for the whole year, indicating poor representation of the surface water budget in SRB. The residual term in ERA-Interim switches from positive to negative from May to September, again showing large uncertainties in ERA-Interim in
20 the associated hydro-climatic variables in SRB. Compared to MRB, the seasonal cycle of ET in SRB in the WRF simulation is more consistent with those in the reanalyses as the maximum ET occurs in July for all datasets.

WRF-CTL simulation captures the peak runoff in spring for SRB (in April) and MRB (in May) as shown in Fig. 3 and 2. Although solar insolation enhances in spring, the prevalence of frozen ground effectively reduces meltwater infiltration (Pomeroy et al., 2007), especially the Noah LSM in WRF tends to overestimate the impermeability of frozen ground. Much of
25 the snowmelt stays on the ground and gives rise to surface saturation and generating substantial runoff, which is especially true for Noah LSM that underestimates the permeability of the frozen soil in the cold regions (Niu and Yang, 2006). Additionally, the storage terms (consisting of soil moisture and snow water equivalent (SWE)) vary among reanalyses and WRF because of the different soil layer depths among the model and the reanalyses. Finally, differences may occur because the depth-to-bedrock information used by different reanalysis products may vary. For ERA-Interim, the simple assumption of no bedrock
30 everywhere has been adopted (Balsamo et al., 2009).

For all the datasets, the predominant terms are P and ET during the warm seasons. P and ET's annual cycles are also more consistent across the datasets, unlike storage, runoff, and residual terms. The residual terms are much smaller in the WRF simulation and NARR, indicating that the components of the budget equation such as P, ET, the change of storage, and runoff

are more balanced in the WRF model and NARR. This indicates large uncertainties in the hydro-climatic variables assimilated by ERA-Interim and JRA-55, as the residual terms are essentially the unbalanced term introduced to the model through assimilation of observation. In winter, P is balanced by the increase of storage as snow and ice; in spring, the change of storage is balanced by the increased runoff and generally P-ET; in summer, P-ET is close to 0, with the change of storage equalling runoff; in autumn, ET decreases more than P does, resulting in the enhanced storage term. Runoff is extremely low in the WRF simulation and the reanalyses since winter snowfall provides little melting over most parts of the basins.

The changes in each component of the water balance equation in WRF-PGW relative to WRF-CTL are shown in Figs. 4 and 5. Compared to WRF-CTL, the amplitudes of the annual cycle of P and ET in both basins are larger in WRF-PGW because of the increases of P and ET in summer, signaling an enhanced water cycle. Both MRB and SRB show a decrease of peak runoff. Runoff in MRB decreases in warm seasons and increases in cold seasons. Runoff in SRB shows a large reduction in April and May and a small increase in November and winter. These changes are due to the fact in a warmer climate ET increases more than P in summer, which causes less water storage is converted to runoff during spring and summer. The peak runoff for SRB also shifts from April in WRF-CTL to June in WRF-PGW. The increase of winter P in MRB exceeds the increase in storage in WRF-PGW, which causes a small increase in winter runoff and a decrease in summer runoff in MRB. The storage change term in SRB shows a significant decrease in summer due to the deficit in P-ET in the future, which also results in a decrease of runoff.
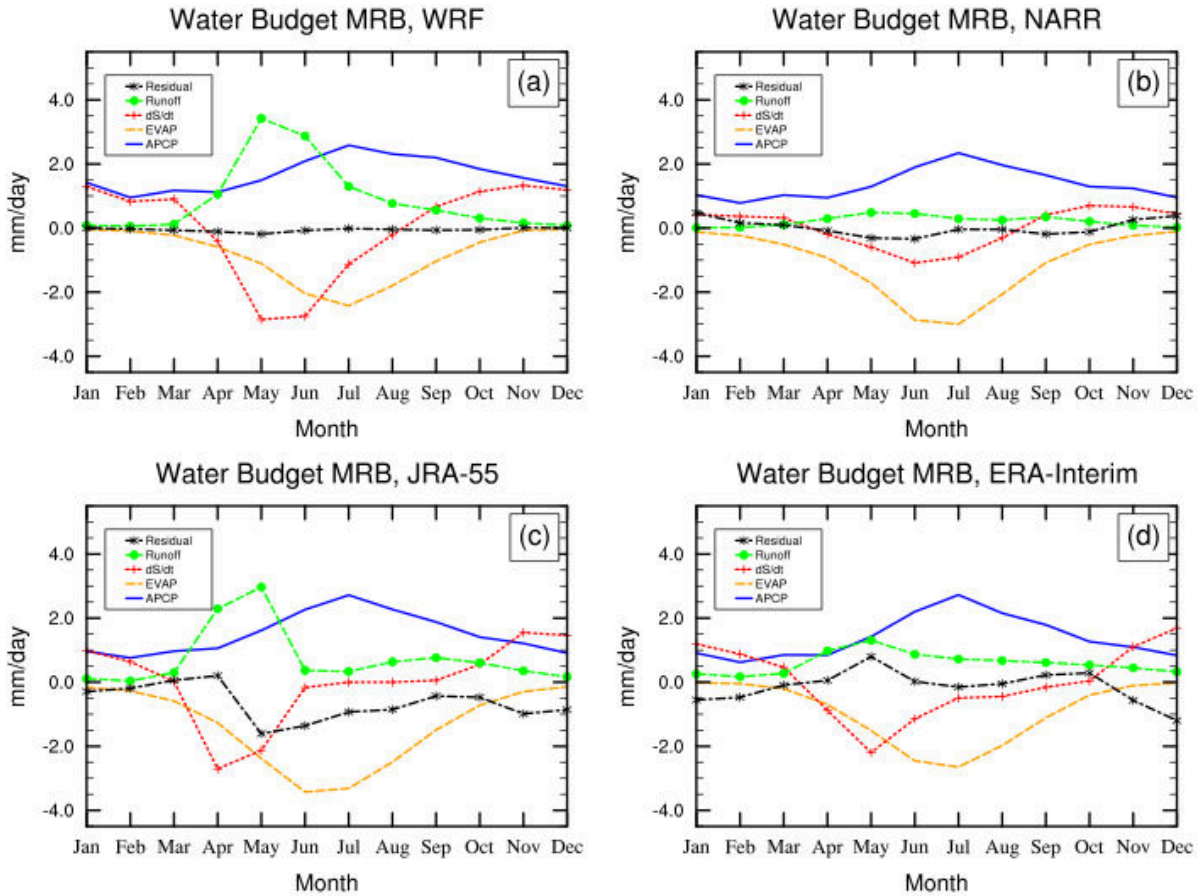
Figure 2. The surface water budget (mm day^{-1}) in MRB from WRF-CTL and the reanalysis datasets: NARR, ERA-Interim, JRA-55. EVAP denotes evapotranspiration. APCP denotes accumulated precipiation per time interval.

3.2 Divergence of Vertically Integrated Moisture Flux

Unlike the surface water budget, which considers the water added to and extracted from the land surface, the general balance equation for atmospheric water vapour considers the water vapour budget for the whole atmospheric column. The general balance equation for atmosphere considers the extraction by P and addition by ET from the underlying surface and convergence 5 or divergence of water vapour through atmospheric transport.

Figure 6 shows the seasonal cycle of the components of surface moisture flux over the two river basins in the WRF simulations. Over winter, spring and autumn, the vapour convergence is much larger in MRB (-0.6-1.2 mm day^{-1}, peaks in October) than in SRB (-0.1-0.9 mm day^{-1}, peaks in April). MRB shows a more balanced P and ET during summer with a small moisture divergence (0.2-0.4 mm day^{-1}) during summer. SRB has a vapour convergence in June (-0.6 mm day^{-1}) and large divergence 10 in July(1.1 mm day^{-1}) and a smaller divergence (0.5 mm day^{-1}). In July and August. Due to the large deficit of P-ET and
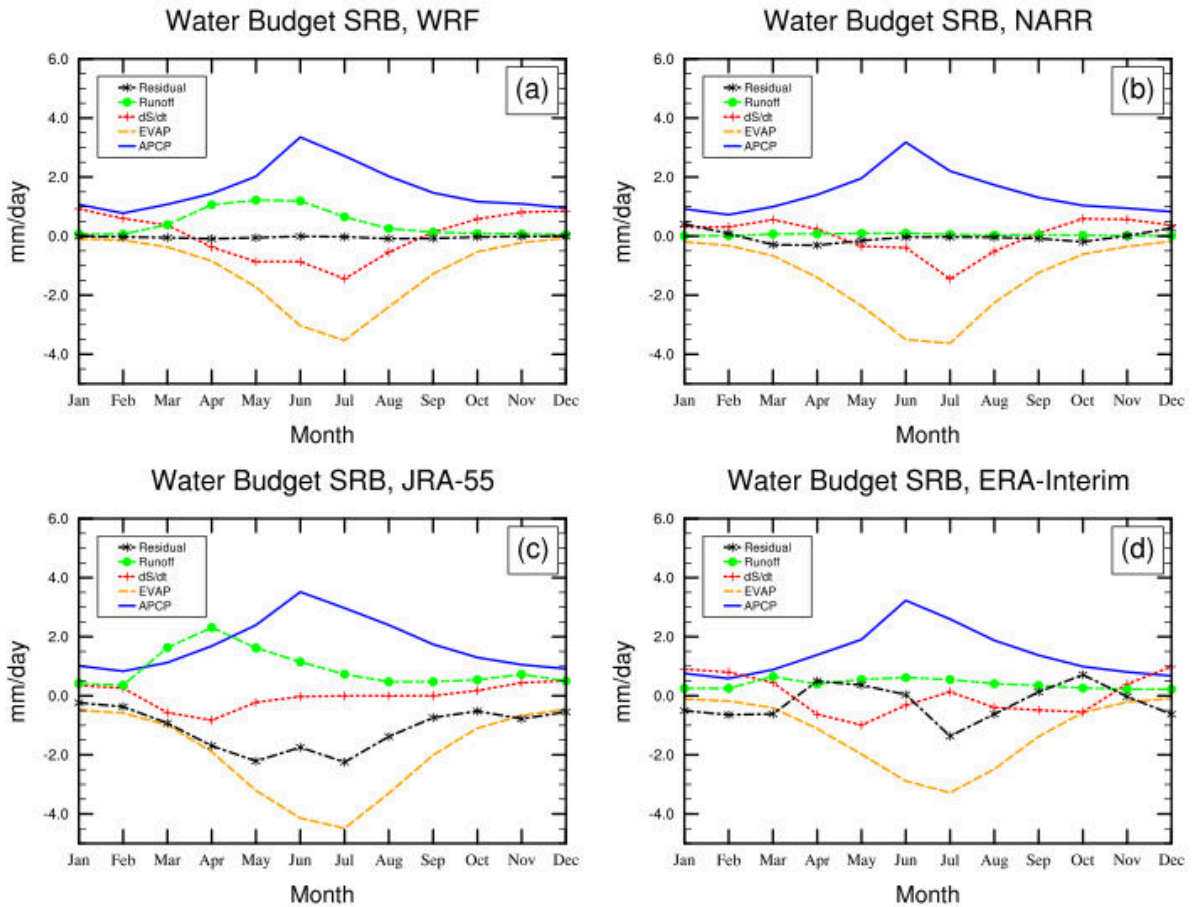
Figure 3. The surface water budget (mm day^{-1}) in SRB from WRF-CTL and the reanalysis datasets: NARR, ERA-Interim, JRA-55. EVAP denotes evapotranspiration. APCP denotes accumulated precipiation per time interval.

positive moisture divergence, more moisture is transported out of the two basins. The residual term in the transitional months reflects the change in water vapor holding capacity: fast warming months correspond to the increases of water vapor in the atmosphere and the positive residual (adding vapor to the air, which is opposite to P). Cooling months correspond to the decreases of water vapor in the atmosphere and the negative residual. The timing of the peak residual terms for MRB in warm

15 seasons is earlier than SRB as MRB starts to cool earlier (in August) than SRB.

The atmospheric water vapor budget in WRF-PGW is also shown in Fig. 6. The seasonal cycles of each component are similar in both WRF-PGW and WRF-CTL. Over winter, spring and autumn, the vapour convergence is much larger in MRB (-1-1.5 mm day^{-1}) than in SRB (-0.1-0.8 mm day^{-1})). MRB shows a more balanced P and ET during summer with a small moisture divergence (0.5-1.0 mm day^{-1}) during summer. Compared to WRF-CTL, ET in both SRB and MRB increases significantly in

20 summer, especially in July. During summer, both MRB and SRB show moisture divergence in the CTL and PGW experiments,
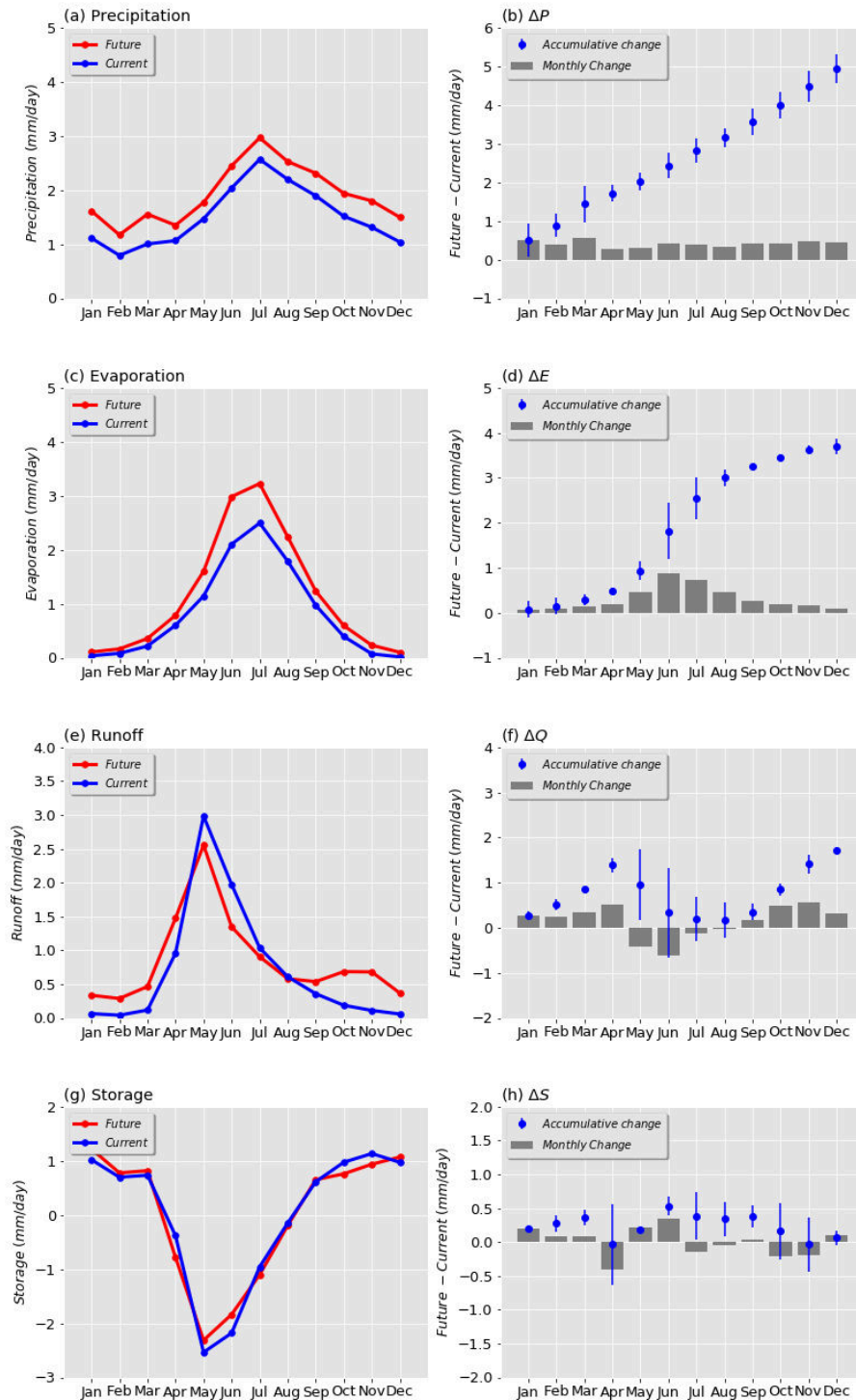
Figure 4. The surface water budget (mm day^{-1}) in MRB for the WRF-CTL and the WRF-PGW simulations: a) P, b) changes in P and its accumulated changes in P; c) ET, d) changes in ET and its accumulated changes in ET; e) runoff, f) changes in runoff and its accumulated changes in runoff; g) storage and h) changes in storage and its accumulated change; g) storage and h) changes in storage and its accumulated change.
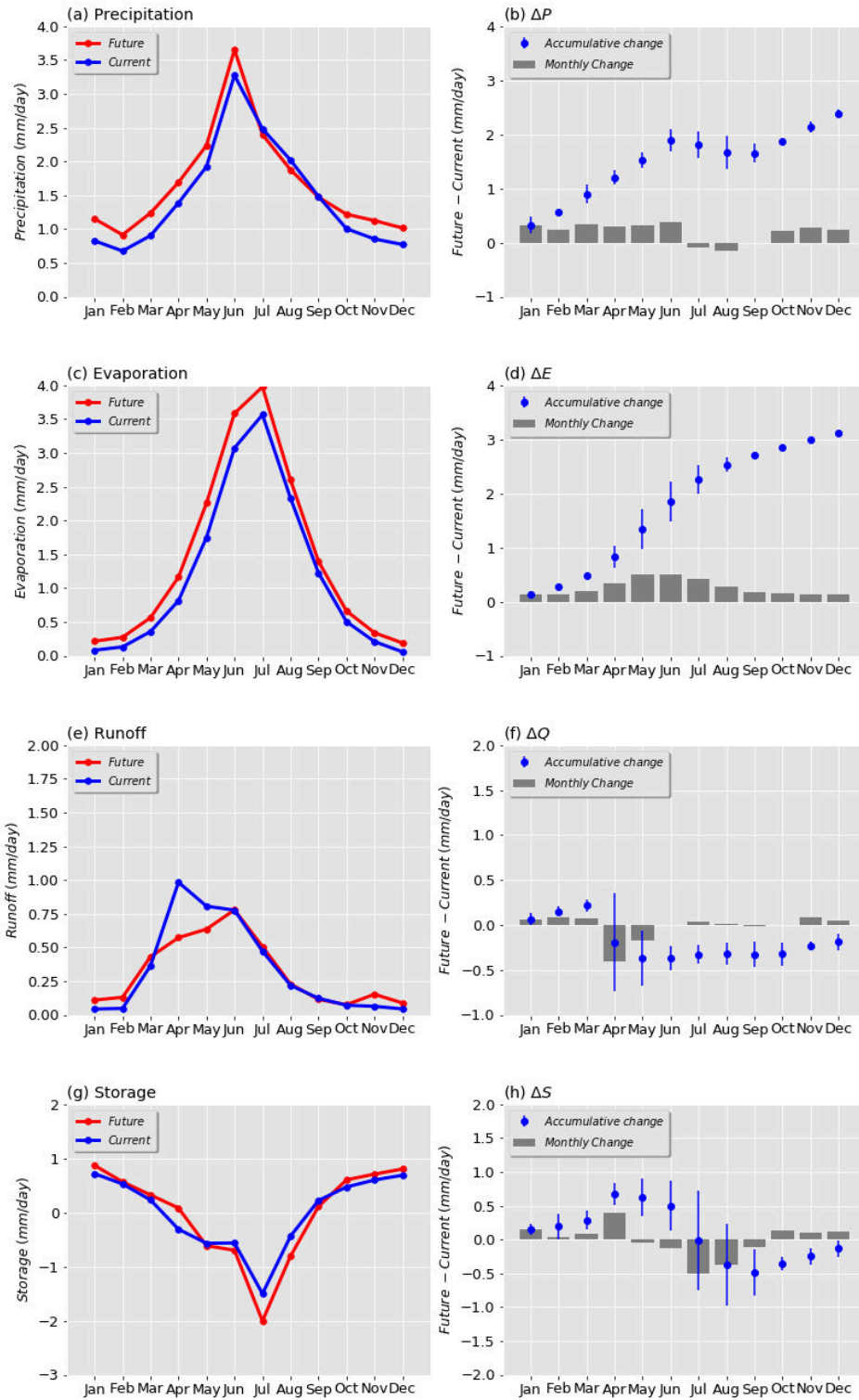
Figure 5. The same as in 4 except for SRB.

as ET is larger than P for each basin. In MRB, the moisture divergence in summer increases from 0.3 mm day^{-1} in WRF-CTL to about 1mm day^{-1} in WRF-PGW, which is consistent with the increase of the deficit of $P - ET$ in WRF-PGW. In SRB, the July moisture divergence in WRF-CTL is about 1mm day^{-1} and increases to about 2mm day^{-1} in WRF-PGW, consistent with the large increases of ET and small changes in P.

25 Unlike MRB, where P is largely balanced by moisture convergence in winter, SRB shows a large residual term in its atmospheric water vapor balance (Fig. 6) in winter. This large residual term in water vapour budget during winter in SRB is due to that a portion of water into the basin is in the form of solids that are transported over the mountain by the westerly. This transport in solid form of water causes a large residual term in the atmospheric water vapor budget, as it is not accounted for as shown in Fig. 6. The cross-mountain/basin transport in condensates either becomes precipitation or melt/sublimates back into

30 water vapour when the air descends and warms adiabatically. This mechanism is consistent with the changes in the solid form of water across the mountain barrier on the western edge of SRB and the increases of moisture in the descent flow of the lower atmosphere on the lee side as shown in Fig. 7. The ice/snow content distribution in the atmosphere is of relatively large quantity ($.025$ g kg^{-1}) concentrated in the lower atmosphere on the windward side of the mountain and close to 0 on the lee side (not shown). The downward motion in the lower part of troposphere over the lee side of the Canadian Rockies is demonstrated

5 by the sharp drop in the potential temperature contour just by the western boundary of SRB corresponding to a significant lower troposphere warming. Accompanying this downward motion is higher temperature and moisture near the western part of SRB. The increase of moisture content in the lower atmosphere on the lee side of the Rockies cannot be accounted for by the moisture content before the adiabatic descent as the moist layer is much thinner over the mountain. The added water vapor comes from the evaporation of ice particles as the air descends and warms as shown by the decease of ice content near 288 K

10 isentrope. Due to this process, the average moisture content and temperature are higher at the mid- and lower levels near the mountain than in further downwind locations. Consistent with the fact is the higher vapour mixing ratio near the Rockies the divergence of water vapour mainly concentrates in the lower 1 km. The upward motion in the upper troposphere overlaying over the downward flow corresponds to a region of large ice mixing ratio over the lee side of the mountain, which is caused by the lifting and cooling related to a mountain wave response (Cotton et al., 2010a). Because topography strongly impacts as-

15 cent/descent and condensation/evaporation, high-resolution regional climate modelling is better suited to represent the process than lower resolution modeling and statistical downscaling.

Changes in atmospheric moisture divergence are presented in Fig. 8. The MRB moisture divergence shows an increase in summer and reductions in winter and autumn, which means more water vapour converges into MRB during cold seasons, and vice versa in summer. The largest increase in moisture divergence in MRB occurs in June when evaporation greatly increases

20 in the eastern MRB and precipitation only increases slightly. The accumulative change of moisture divergence decreases on throughout the year in MRB. The SRB moisture divergence shifts from increasing during warm months (May-September) to little change over cold months. The maximum changes in divergence over SRB occur in July. The annual accumulative change in the moisture flux over SRB shows an enhanced divergence of about 2 mm day^{-1}, which is mainly driven by the large accumulative increase of ET over SRB. Little changes occur in storage during cold season in SRB until spring (April,

25 May) when higher precipitation in PGW causes larger water storage in the land surface. The increase of vapour divergence in summer is supplied by a larger draw-down in soil moisture and reduction in run-off. The vertical profile of atmospheric vapour divergence (not shown) shows that the majority of the increase of the divergence occurs below 850 hPa.
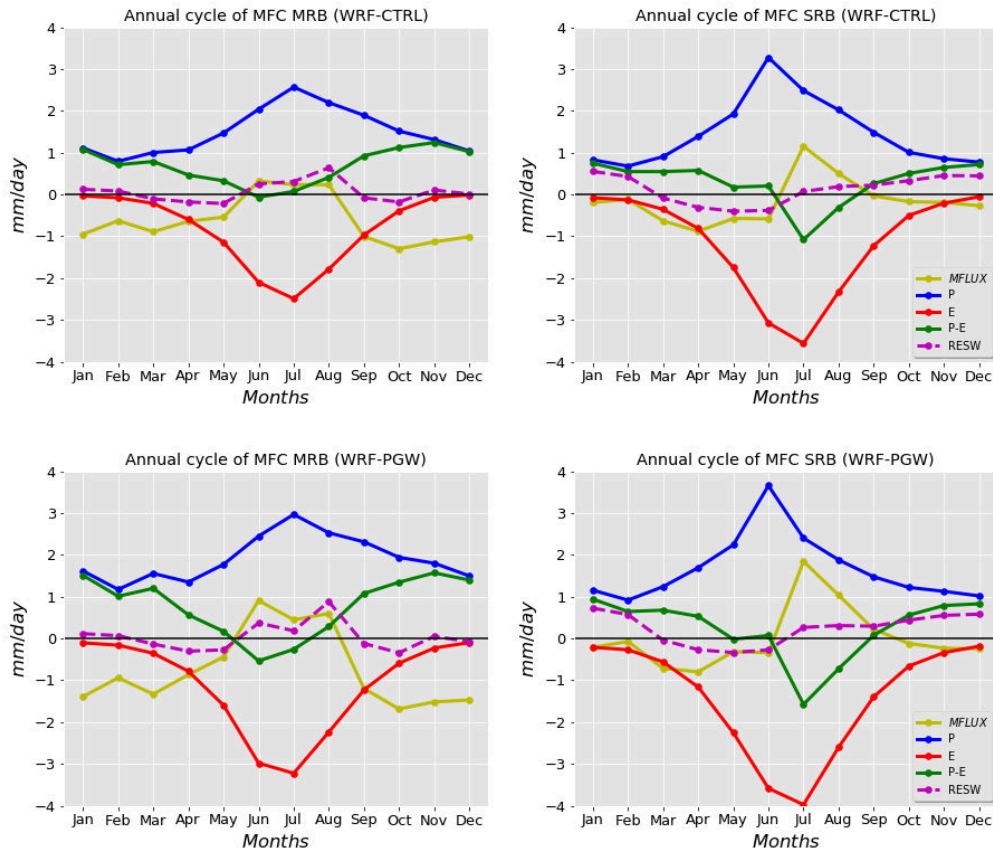
Figure 6. Atmospheric water vapour budget (mm day^{-1}) in WRF-CTL (top) and WRF-PGW (bottom) in MRB (left) and SRB (right). MFLUX stands for vertically integrated moisture flux convergence.
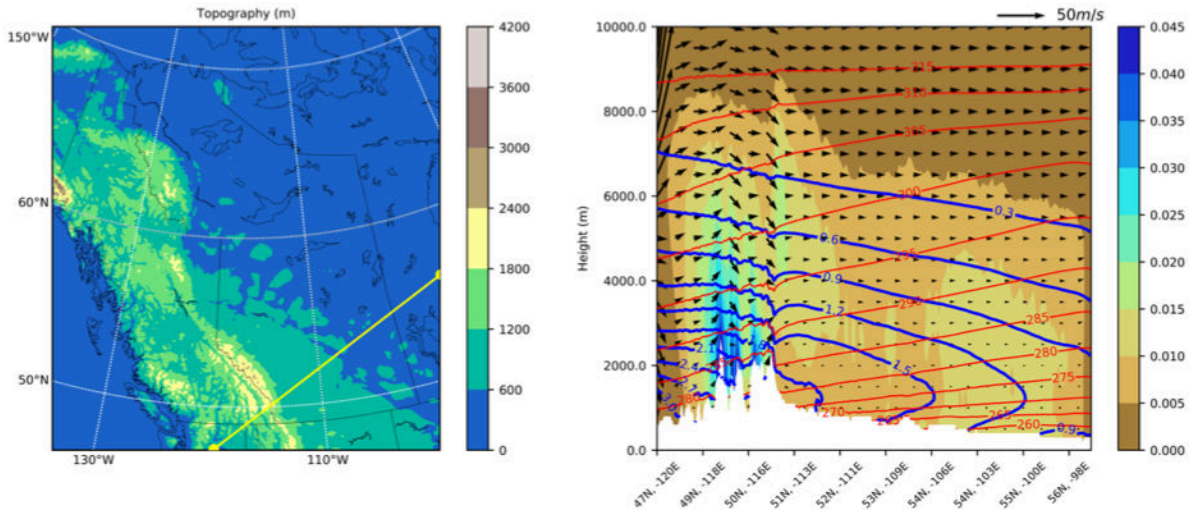
Figure 7. Topography (m) in Western Canada. (b) Cross-section of potential temperature (K, thin red contour), water vapor mixing ratio (g kg-1, thick blue contour), the sum of snow, ice and graupel mixing ratio (g kg-1, shading), and winds (m s-1) perpendicular to the Canadian Rockies at 115W, 50N in December. The vertical component of winds is scaled by 100 for illustration purposes.

3.3 Distribution of Precipitation, Evapotranspiration and Moisture Divergence

Figures 9 - 12 show the spatial distribution of precipitation, ET, atmospheric moisture divergence, and soil moisture terms for both WRF-CTL and WRF-PGW. The increase of P (precipitation) and ET (evapotranspiration) in PGW is the most predominant features in all months, indicating the water cycle, the water exchange between the land and the atmosphere, becomes stronger in a warmer future.

As shown in Fig. 9, the major increase of P extends from the Canadian Rockies northeastward and covers mainly the MRB and Nelson river basin in March. Due to general warming in the domain, ET is also enhanced across the domain, especially in British Columbia and near the eastern end of SRB. Soil moisture shows a large reduction in British Columbia and a large increase over central and eastern Saskatchewan, where the increase in ET is larger than the increase in P. This increase of soil moisture in the Prairies is beneficial to the agriculture as the growing seasons in a warmer climate may be advanced to April. The moisture flux shows an increase of divergence in the southern Prairies and an enhancement of convergence over MRB, which corresponds to the spatial distribution of the change in P over these regions.

Figure 10 shows P increases across the domain, with a strong magnitude over the Pacific coast and the northern mountainous regions in May. This strengthening in P is countered by the increased ET, especially in the southern domain, which generates a reduction of soil moisture over large regions in the south and west covering British Columbia, southern MRB, and SRB. The decrease of soil moisture in May is due to earlier snowmelt and increased evaporation demand in the warmer future. The deficit
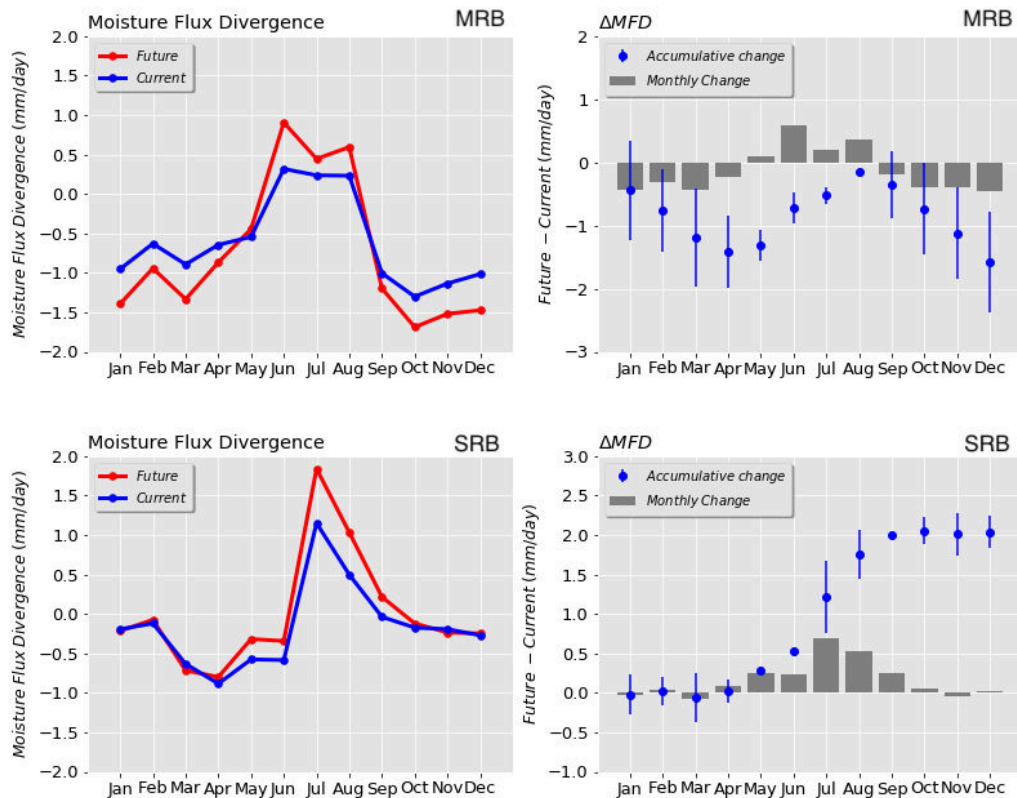
Figure 8. Changes in atmospheric water vapour divergence (mm day^{-1}) for each calendar month between WRF-PGW and WRF-CTL over MRB (top) and SRB (bottom).

of P over ET corresponds to stronger atmospheric moisture divergence in MRB than that in SRB. In general, PGW presents a drier condition for the major agricultural regions compared to CTL in the early growing season.

In July, a general increase of P is shown over most of the domain in WRF-PGW except the southern region, especially near the eastern part of SRB, as shown in Fig. 11. The decrease of soil moisture in the antecedent spring months may contribute to the lack of precipitation increase in PGW in these regions. Compared to May, the increase of ET is more widespread and shifted northward. With this P and ET configuration, the soil moisture substantially decreases in SRB, southwest MRB, and the region close to Hudson Bay. The enhanced ET and unchanged P correspond to an increase of divergence of atmospheric water vapor over SRB, consistent with Fig. 6. Like in May, the soil moisture decreases in the major agricultural regions in Saskatchewan and Alberta, which provides water for the extra evaporation.

At the end of the growing season and early autumn,Figure 12 shows that the WRF-PGW simulation shows a large increase of precipitation near the Pacific coast and the northeast part of the domain; a small decrease of precipitation occurs in SRB. The ET enhancement is the largest near the eastern edge of MRB and SRB. The increase of precipitation is larger than that
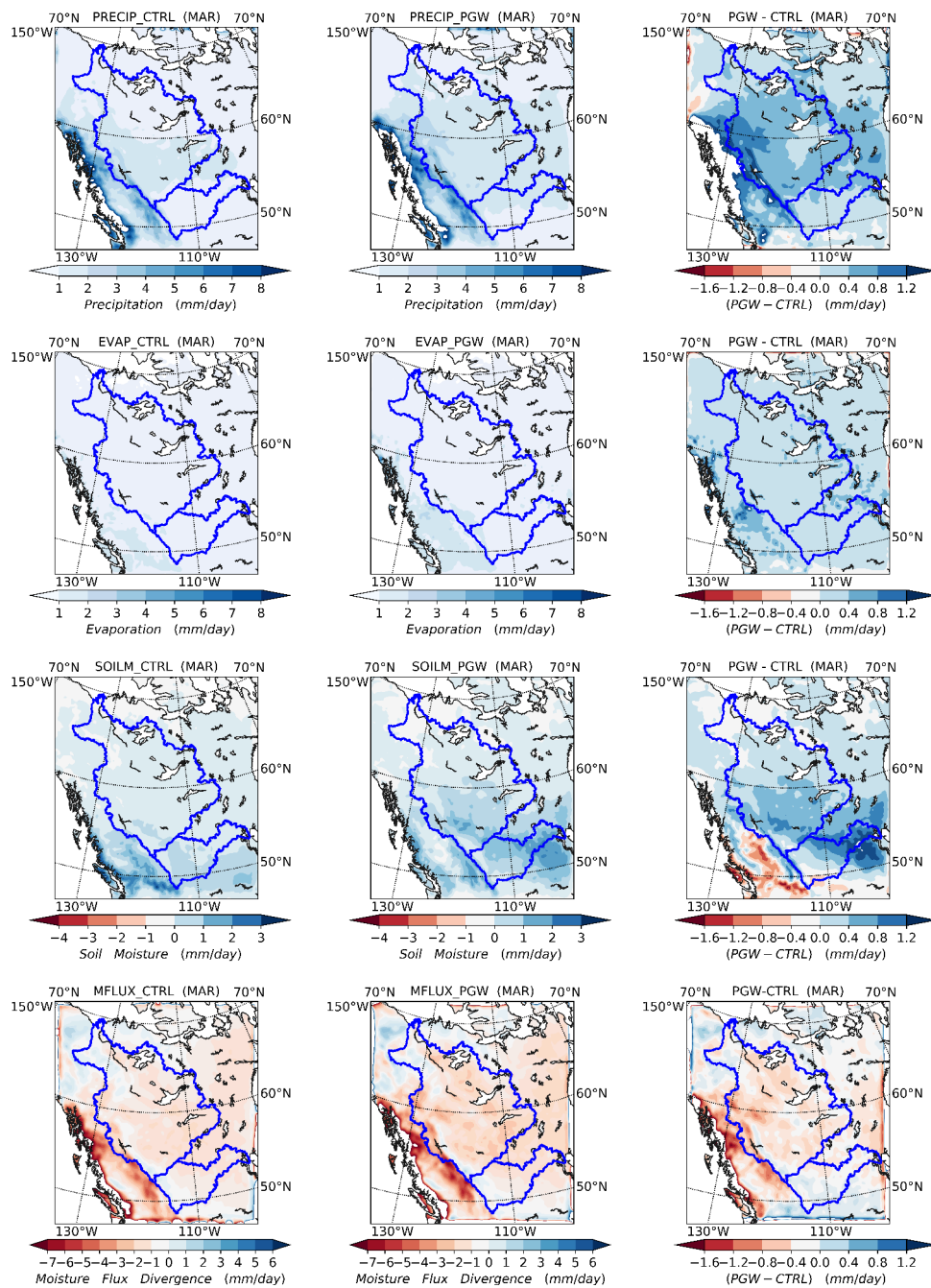
Figure 9. P, ET, changes in soil moisture, and divergence of vertically integrated moisture flux for WRF-CTL (left), WRF-PGW (middle), and differences between WRF-CTL and WRF-PGW (right) in March. The unit of all variables is turned into mm day^{-1}, which makes it easy for comparisons among variables. All variables are averaged over the simulation period over the calendar month.
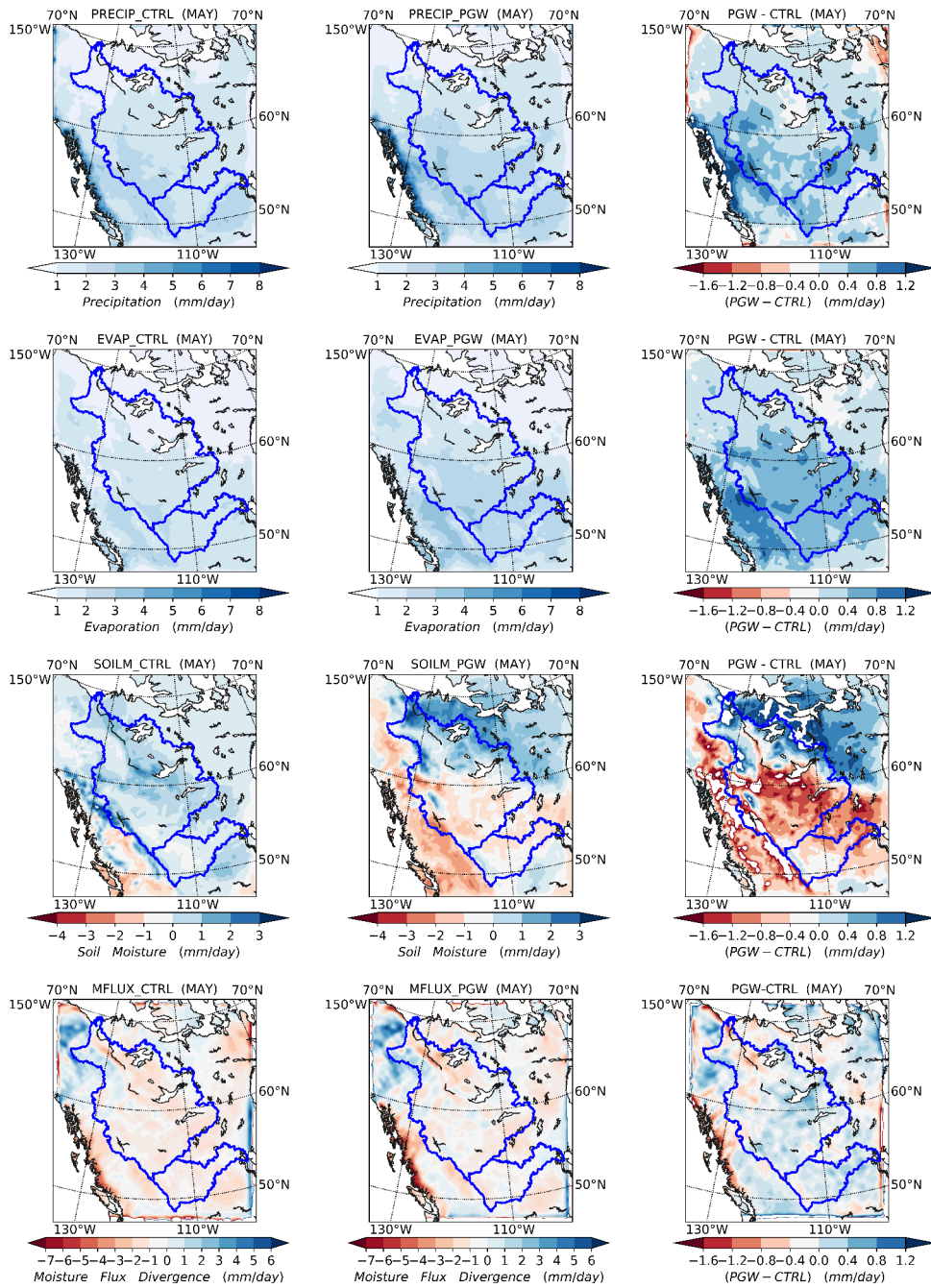
Figure 10. Same as in Fig. 9, except for May.
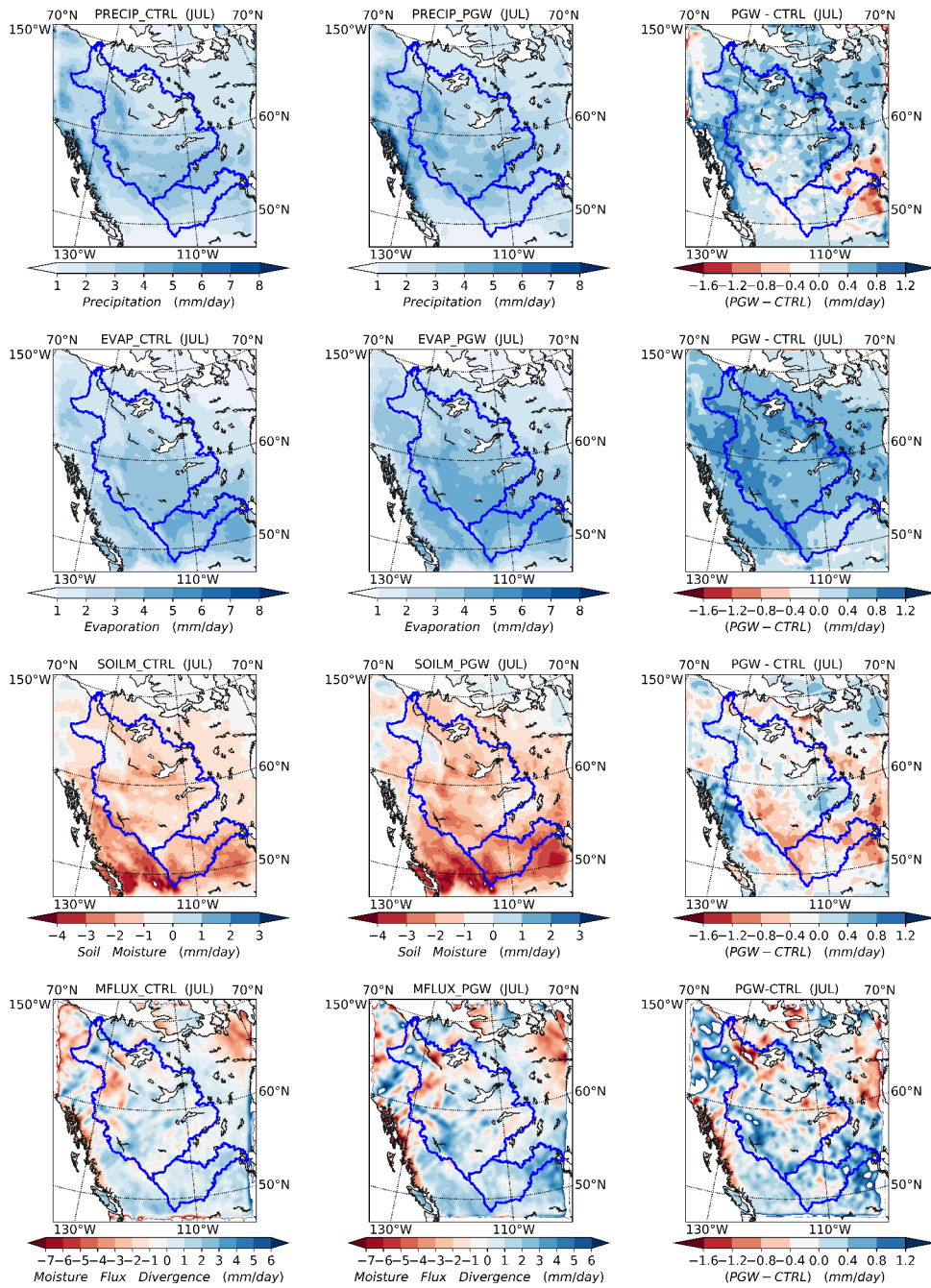
Figure 11. Same as in Fig. 9, except for July.
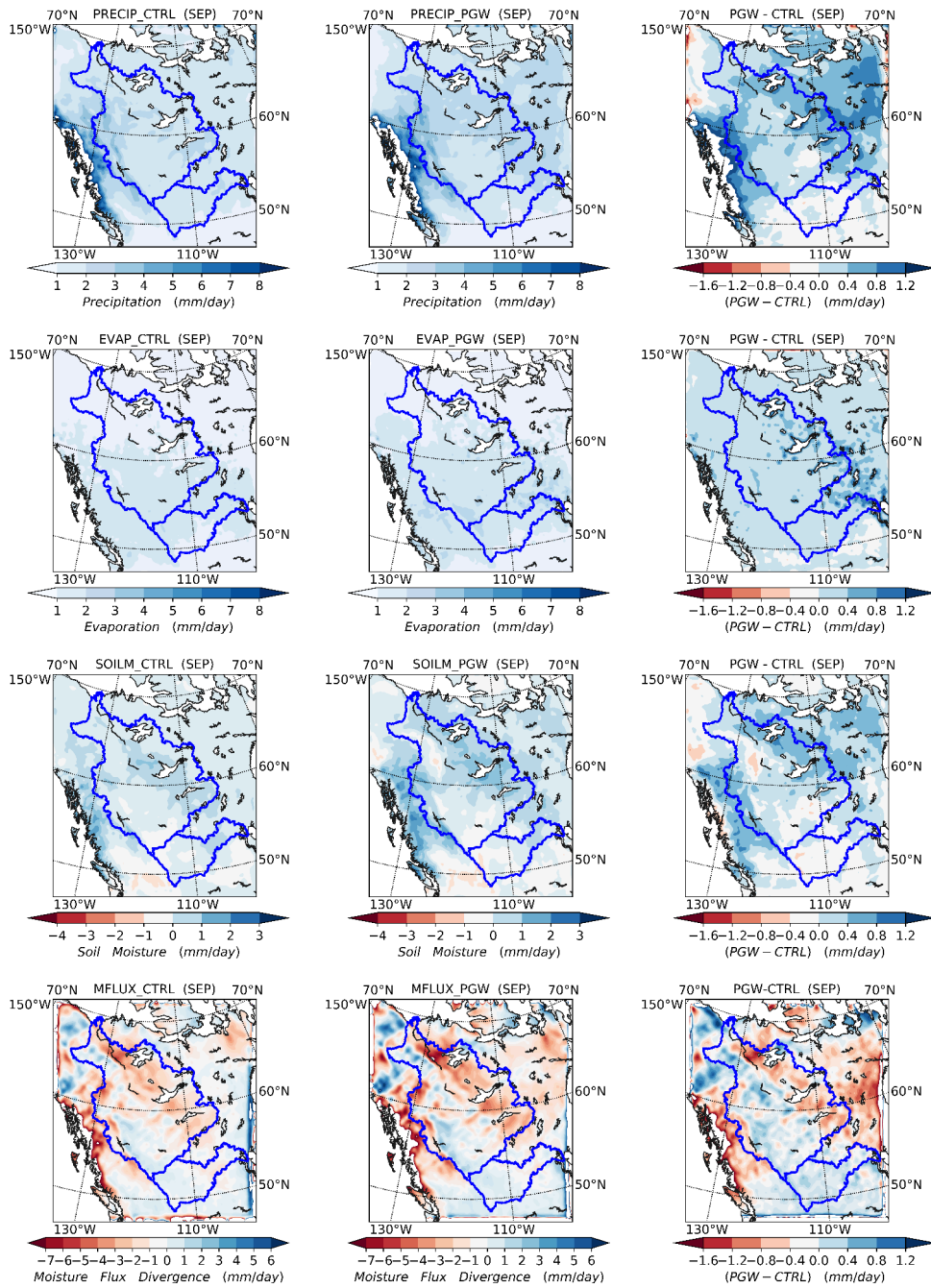
Figure 12. Same as in Fig. 9, except for September.

of ET for MRB, the BC coastal region, and the northeast corner of the domain, where large increases of soil moisture occur. The convergence of atmospheric water vapour increases in the northeast and eastern parts of MRB, which matches well with increases in P and ET. Conversely, the increase of divergence of moisture flux over western MRB and SRB is due to the decreases of $P - ET$.

5   Over the course of the year, the atmosphere provides a net influx of water vapour for the two river basins through moisture convergence during spring, autumn, and winter. In summer, the excess of ET - P over the two basins is balanced by moisture divergence over the regions and by the residual term (the decreases of precipitable water) in MRB. Compared to WRF-CTL, PGW's water vapour exchange between land and atmosphere shows an increased water cycling through enhanced P and ET throughout the year. Higher temperatures allow more water vapour in the atmosphere, thus more water vapor transportation from the Pacific and the Gulf of Mexico. Due to the spatial and temporal heterogeneity of the changes in P and ET, the changes in atmospheric and surface water balance vary over the two basins.

4   Discussion

We have investigated the water balance in the WRF simulations and the reanalyses from two perspectives: the surface water
5   budget and the atmospheric moisture budget. Moisture divergence is affected by two factors: water vapour distribution and atmospheric flow. Convergence of wind can generate moisture flux convergence in a constant field of moisture distribution. Sharp gradients of moisture can also cause large fluxes of moisture without convergence of wind.

The surface water budgets in the model and reanalyses are strongly affected by the representation of the hydrometeorological processes involved in the surface water balance equations. Each reanalysis dataset has different magnitudes of biases in the
10   P, ET, runoff, and water storage terms, depending on geographic locations and seasons. Due to the large uncertainty in model diagnostic terms (i.e. not directly constrained by observation) such as precipitation and evapotranspiration, great caution needs to be exerted when using hydrological variables from reanalyses (Trenberth et al., 2011). Furthermore, the assimilation system of reanalyses have to adjust the model variables according to newly available observation, though water vapour is constrained by satellite observation, the dry air mass or water balance is not strongly constrained (Takacs et al., 2016). In general, the
15   results here show that the model simulation and reanalyses with higher resolution are more inclined to close the surface water budget with minimum residual terms.

In addition to the atmospheric forcing, the generation of runoff through LSMs can further introduce discrepancies in the runoff among models. Though Noah LSM, JRA-55's land surface model SiB and ERA-Interim's TESSEL calculate runoff using similar algorithms, their treatments of landcover and soil can make big differences in runoff generation. Additionally, the land
20   surface in reanalyses are periodically forced by observation at the screen level through assimilation, which could introduce imbalance. Noah LSM has four soil layers with monthly changing leaf area index (LAI) with diverse soil type and land cover. JRA-55's Simple Biosphere model provides three layers of soil with varied depth depending on 13 land cover types. TESSEL is the most crude model in terms of the treatment in the soil and vegetation cover. TESSEL has fixed LAI throughout the year

and only one soil type across the globe, which has been shown to introduce biases in near-surface temperature biases among
25   other deficiencies over the Canadian Prairies (Betts and Beljaars, 2017).

Although P generally increases throughout the domain in WRF-PGW compared to WRF-CTL in summer, it substantially decreases in the eastern part of SRB and surrounding region in July. In the summer months (June, July, and August), SRB experiences no increase or only a slight decrease of P in the WRF-PGW simulation compared to WRF-CTL. The reason for the decrease of P in eastern SRB is unclear and further investigation is needed to figure out the cause of the decrease
30   of summer P in the region. An examination of the atmospheric circulation differences in the forcing field of WRF-PGW compared to WRF-CTL in the lower atmosphere showed a decreased westerly mean wind at 750 hPa and 500 hPa in response to the reduced meridional thermal gradient across SRB in summer. We found that changes in WRF-PGW circulation caused by accumulated differences in the WRF simulated mesoscale processes are much different from the forcing field and depend on the internal atmospheric and terrestrial processes (Li et al., 2019). Indeed, the WRF-PGW large scale forcing caused shifts in mean flow, but changes in horizontal and vertical transport of heat and moisture also depend on the responses of the mesoscale to local-scale processes. This dynamical feedback again shows the importance of high-resolution dynamical downscaling both
5   to represent the unresolved processes by producing a fine-scale realization of hydroclimatic processes and to properly produce the accumulated effects on the large-scale fields.

From the atmospheric water vapour balance perspective, convergence and divergence of the vertically integrated moisture flux are essentially the differences between P and ET in winter and summer when changes in air temperature are relatively small. A region with mean excess (deficit) of P over ET corresponds to convergence (divergence) of moisture flux. Therefore, both
10   MRB and SRB are water vapour divergence regions in summer because their ET exceeds P. As the summer precipitation over SRB and MRB are mostly related to convections, the middle and upper troposphere above these two regions is wetter than their counterparts west of the Rockies due to the vertical transport of moisture by convections. The blocking effects of the Cordillera on the westerly moisture flux suppress the net moisture convergence in the Basin throughout the year. The basin on the whole remains as a moisture sink. As surface evaporation is extremely weak, winter P is largely balanced by the large-scale moisture
15   convergence in the basin in MRB.

Moisture convergence is associated with stronger P-ET; however, the convergence is not the driving factor. In fact, weather systems such as extratropical cyclones are responsible for the bulk transfer of heat (vapor as a form of latent heat) meridionally to balance the excess (deficit) of solar heating in low (high) latitudes, and deep convections transfer heat and moisture between the lower and upper atmosphere (Cotton et al., 2010b). MRB and SRB are situated in an area where polar fronts fluctuate with
20   passing extratropical cyclones. During winter over the Canadian Prairies, the polar front zone locates in MRB more often than in SRB with less orographic barriers. Therefore, the moisture flux into MRB and P over MRB are larger than those over SRB (Fig. 6).

In the PGW simulation, the water recycling rate increases at seasonal and sub-seasonal scales. On the one hand, during cold seasons the increase of P and storage is supplied by the enhanced atmospheric moisture convergence as atmospheric vapour

loading increases. The increased storage in snow cover and soil moisture provides the excessive evaporation demand during warm seasons in PGW simulation compared to CTL. On the other hand, during the warm season, the increased evaporation corresponds to an increased divergence of atmospheric vapour flux out of MRB and SRB, especially at the lower troposphere, which means more stored water and concurrent precipitation are recycled back into the atmosphere. Due to the net export of water vapour from both basins, the downwind regions of MRB and SRB get more water vapour flux in PGW than in CTL.

5   Conclusions

For the surface water budget, the high-resolution WRF simulation shows a significantly lower residual than the reanalysis datasets though each component of the water cycle has its bias relative to station observation. Among the reanalysis datasets, NARR has the lowest residual term. Runoffs in NARR and ERA-Interim are too small compared to observations due to their large overestimation of ET. Changes in the surface water budget simulated by WRF show an enhanced water cycle throughout the year. The enhanced ET causes soil moisture to decrease through summer, with the largest decreases moving in tandem with the band of the strongest increases in ET. As a result, at the beginning of the growing season (May) the soil moisture content is lower in the Canadian Prairies in WRF-PGW than in WRF-CTL.

There is significant difference between the water balance of MRB and SRB due to their geographic features. For atmospheric water budget, during winter P is balanced by the residual term in SRB. However, in MRB, P-ET is balanced by moisture divergence. The difference of this budget between the two basins is caused by the cross-mountain transport through descending flow with a large quantity of ice particles. This descending flow over the lee slope often occurs over the SRB's western boundary. As the prevailing westerly airflow ascends on the west side of the Rockies, water vapour cools and freezes to ice crystals that contribute to precipitation. The remainder is transported over the mountain into the SRB as ice in the air. This is an important part of water budget that can only be faithfully simulated with high-resolution topography.

Future changes in water cycle as indicated by WRF-PGW (RCP8.5) and WRF-CTL show a general enhancement of water cycle in both basins. The recycling rate of water is larger when more water vapour is coming from local evaporation than atmospheric transport for precipitation generation. Therefore, for both MRB and SRB the recycling rates are larger in PGW simulations as both basins have much larger evaporation increases in summer than P with increases in column vapour divergence (water vapour going out of the basins). For MRB, precipitation and evaporation increase in warm seasons consistently. Thus, for MRB more moisture from local evaporation, more precipitation. For MRB, the change in soil moisture is small and evaporation is mostly recycling of precipitation. The precipitation increases from May to June for SRB but decreases in July and August; the evaporation increases in all months and moisture divergence increases in warm season. For SRB, the increase of evaporation is at the sacrifice of soil moisture, canopy water etc.(storage from earlier months) in July and August, which could partly explain the decrease in precipitation.

High-resolution regional climate modeling provides indispensable insights into the hydroclimatic processes that are critical to the water cycle over SRB and MRB. This study shows further work using CP RCMs is important for enhancing the understanding and accurate projections of the impact of climate change on the water cycle in the region.

Acknowledgement. The authors gratefully acknowledge the support from the Changing Cold Regions Network (CCRN) funded by the Natural Science and Engineering Research Council of Canada (NSERC), as well as the Global Water Future (GWF) project and Global Institute of Water Security (GIWS) at University of Saskatchewan. Yanping Li acknowledge the support from NSERC Discovery Grant.

References

Balsamo, G., Beljaars, A., Scipal, K., Viterbo, P., van den Hurk, B., Hirschi, M., and Betts, A. K.: A Revised Hydrology for the Ecmwf Model: Verification From Field Site To Terrestrial Water Storage and Impact in the Integrated Forecast System, Journal of Hydrometeorology, 10, 623–643, https://doi.org/10.1175/2008jhm1068.1, https://doi.org/10.1175/2008jhm1068.1, 2009.

5 Betts, A. K. and Beljaars, A. C. M.: Analysis of Near-surface Biases in Era - I Nterim Over the C Anadian P Rairies, Journal of Advances in Modeling Earth Systems, 9, 2158–2173, https://doi.org/10.1002/2017ms001025, https://doi.org/10.1002/2017ms001025, 2017.

Chen, F. and Dudhia, J.: Coupling an Advanced Land Surface-Hydrology Model With the Penn State-Ncar Mm5 Modeling System. Part I: Model Implementation and Sensitivity, Monthly Weather Review, 129, 569–585, https://doi.org/10.1175/1520-0493(2001)129<0569:CAALSH>2.0.CO;2, https://doi.org/10.1175/1520-0493(2001)129$<$0569:CAALSH>2.0.CO;2, 2001.

10 Collins, W. D., Rasch, P., Boville, B., Hack, J., McCaa, J., Williamson, D., Kiehl, J., Briegleb, B., Bitz, C., Lin, S.-J., Zhang, M., and Dai, Y.: Description of the NCAR Community Atmosphere Model (CAM 3.0), Tech. rep., Natl. Cent. for Atmos. Res., Boulder, Colorado, NCAR Technical Note/TN464+STR, 2004.

Cotton, W. R., Bryan, G., and Van den Heever, S. C.: The Influence of Mountains on Airflow, Clouds, and Precipitation, vol. 99 of *International Geophysics Series*, chap. 11, pp. 673–750, Academic press, 2 edn., 2010a.

15 Cotton, W. R., Bryan, G., and Van den Heever, S. C.: Storm and cloud dynamics, vol. 99, Academic press, 2010b.

Dee, D., Uppala, S., Simmons, A., Berrisford, P., Poli, P., Kobayashi, S., Andrae, U., Balmaseda, M. A., Balsamo, G., Bauer, P., Bechtold, P., Beljaars, A., van de Berg, L., Bidlot, J.-R., Bormann, N., Delsol, C., Dragani, R., Fuentes, M., Geer, A., Haimberger, L., Healy, S., Hersbach, H., Hólm, E. V., Isaksen, L., Kållberg, P., Köhler, M., Matricardi, M., McNally, A., Monge-Sanz, B., Morcrette, J.-J., Peubey, C., Rosnay, P. D., Tavolato, C., Thepaut, J.-J., and Vitart, F.: The ERA-Interim reanalysis: Configuration and performance of the data 20 assimilation system – This report is superseded by the version published in Q J Roy Meteor Soc., Shinfield Park, Reading, 2011.

Deser, C., Phillips, A., Bourdette, V., and Teng, H.: Uncertainty in Climate Change Projections: the Role of Internal Variability, Climate Dynamics, 38, 527–546, https://doi.org/10.1007/s00382-010-0977-x, https://doi.org/10.1007/s00382-010-0977-x, 2012.

Ebita, A., Kobayashi, S., Ota, Y., Moriya, M., Kumabe, R., Onogi, K., Harada, Y., Yasui, S., Miyaoka, K., Takahashi, K., and et al.: The Japanese 55-year Reanalysis "Jra-55": an Interim Report, SOLA, 7, 149–152, https://doi.org/10.2151/sola.2011-038, https://doi.org/10.2151/sola.2011-038, 2011.

25 Hong, S.-Y., Noh, Y., and Dudhia, J.: A New Vertical Diffusion Package With an Explicit Treatment of Entrainment Processes, Monthly Weather Review, 134, 2318–2341, https://doi.org/10.1175/mwr3199.1, https://doi.org/10.1175/mwr3199.1, 2006.

Hwang, Y.-T. and Frierson, D. M. W.: Increasing Atmospheric Poleward Energy Transport With Global Warming, Geophysical Research Letters, 37, n/a–n/a, https://doi.org/10.1029/2010gl045440, https://doi.org/10.1029/2010gl045440, 2010.

30 IPCC: Climate Change 2013: The Physical Science Basis. Contribution of Working Group I to the Fifth Assessment Report of the Intergovernmental Panel on Climate Change, Cambridge University Press, Cambridge, United Kingdom and New York, NY, USA, https://doi.org/10.1017/CBO9781107415324, www.climatechange2013.org, 2013.

Kobayashi, S., Ota, Y., Harada, Y., Ebita, A., Moriya, M., Onoda, H., Onogi, K., Kamahori, H., Kobayashi, C., Endo, H., and et al.: The Jra-55 Reanalysis: General Specifications and Basic Characteristics, Journal of the Meteorological Society of Japan. Ser. II, 93, 5–48, 35 https://doi.org/10.2151/jmsj.2015-001, https://doi.org/10.2151/jmsj.2015-001, 2015.

Koren, V., Schaake, J., Mitchell, K., Duan, Q.-Y., Chen, F., and Baker, J.: A Parameterization of Snowpack and Frozen Ground Intended for Ncep Weather and Climate Models, Journal of Geophysical Research: Atmospheres, 104, 19 569–19 585, 1999.

Li, Y., Li, Z., Zhang, Z., Chen, L., Kurkute, S., Scaff, L., and Pan, X.: High-Resolution Regional Climate Modeling and Projection Over Western Canada Using a Weather Research Forecasting Model With a Pseudo-Global Warming Approach, Hydrology and Earth System Sciences, 23, 4635–4659, https://doi.org/10.5194/hess-23-4635-2019, https://www.hydrol-earth-syst-sci.net/23/4635/2019/, 2019.

Liu, J. and Stewart, R. E.: Water Vapor Fluxes Over the Saskatchewan River Basin, Journal of Hydrometeorology, 4, 944–959, https://doi.org/10.1175/1525-7541(2003)004<0944:WVFOTS>2.0.CO;2, https://doi.org/10.1175/1525-7541(2003)004$<$0944:WVFOTS>2.0.CO;2, 2003.

MacDonald, M. K., Pomeroy, J. W., and Essery, R. L.: Water and Energy Fluxes Over Northern Prairies As Affected By Chinook Winds and Winter Precipitation, Agricultural and Forest Meteorology, 248, 372–385, https://doi.org/10.1016/j.agrformet.2017.10.025, https://doi.org/10.1016/j.agrformet.2017.10.025, 2018.

Mesinger, F., DiMego, G., Kalnay, E., Mitchell, K., Shafran, P. C., Ebisuzaki, W., Jović, D., Woollen, J., Rogers, E., Berbery, E. H., and et al.: North American Regional Reanalysis, Bulletin of the American Meteorological Society, 87, 343–360, https://doi.org/10.1175/bams-87-3-343, https://doi.org/10.1175/bams-87-3-343, 2006.

Niu, G.-Y. and Yang, Z.-L.: Effects of Frozen Soil on Snowmelt Runoff and Soil Water Storage At a Continental Scale, Journal of Hydrometeorology, 7, 937–952, https://doi.org/10.1175/jhm538.1, https://doi.org/10.1175/jhm538.1, 2006.

Pachauri, R. K., Allen, M. R., Barros, V. R., Broome, J., Cramer, W., Christ, R., Church, J. A., Clarke, L., Dahe, Q., Dasgupta, P., Dubash, N. K., Edenhofer, O., Elgizouli, I., Field, C. B., Forster, P., Friedlingstein, P., Fuglestvedt, J., Gomez-Echeverri, L., Hallegatte, S., Hegerl, G., Howden, M., Jiang, K., Cisneroz, B. J., Kattsov, V., Lee, H., Mach, K. J., Marotzke, J., Mastrandrea, M. D., Meyer, L., Minx, J., Mulugetta, Y., O'Brien, K., Oppenheimer, M., Pereira, J. J., Pichs-Madruga, R., Plattner, G.-K., Pörtner, H.-O., Power, S. B., Preston, B., Ravindranath, N. H., Reisinger, A., Riahi, K., Rusticucci, M., Scholes, R., Seyboth, K., Sokona, Y., Stavins, R., Stocker, T. F., Tschakert, P., van Vuuren, D., and van Ypserle, J.-P.: Climate Change 2014: Synthesis Report. Contribution of Working Groups I, II and III to the Fifth Assessment Report of the Intergovernmental Panel on Climate Change, IPCC, Geneva, Switzerland, 2014.

Pithan, F. and Mauritsen, T.: Arctic Amplification Dominated By Temperature Feedbacks in Contemporary Climate Models, Nature Geoscience, 7, 181–184, https://doi.org/10.1038/ngeo2071, https://doi.org/10.1038/ngeo2071, 2014.

Pomeroy, J. W., Gray, D. M., Brown, T., Hedstrom, N. R., Quinton, W. L., Granger, R. J., and Carey, S. K.: The Cold Regions Hydrological Model: a Platform for Basing Process Representation and Model Structure on Physical Evidence, Hydrological Processes, 21, 2650–2667, https://doi.org/10.1002/hyp.6787, https://doi.org/10.1002/hyp.6787, 2007.

Prein, A. F., Langhans, W., Fosser, G., Ferrone, A., Ban, N., Goergen, K., Keller, M., Tölle, M., Gutjahr, O., Feser, F., Brisson, E., Kollet, S., Schmidli, J., van Lipzig, N. P. M., and Leung, R.: A Review on Regional Convection-Permitting Climate Modeling: Demonstrations, Prospects, and challenges, Rev Geophys, 53, 323–361, https://doi.org/10.1002/2014RG000475, https://doi.org/10.1002/2014RG000475, 2015.

Rasmussen, R., Liu, C., Ikeda, K., Gochis, D., Yates, D., Chen, F., Tewari, M., Barlage, M., Dudhia, J., Yu, W., Miller, K., Arsenault, K., Grubišić, V., Thompson, G., and Gutmann, E.: High-Resolution Coupled Climate Runoff Simulations of Seasonal Snowfall Over Colorado: A Process Study of Current and Warmer Climate, Journal of Climate, 24, 3015–3048, https://doi.org/10.1175/2010JCLI3985.1, https://doi.org/10.1175/2010JCLI3985.1, 2011.

Rasmussen, R., Ikeda, K., Liu, C., Gochis, D., Clark, M., Dai, A., Gutmann, E., Dudhia, J., Chen, F., Barlage, M., Yates, D., and Zhang, G.: Climate Change Impacts on the Water Balance of the Colorado Headwaters: High-Resolution Regional Climate Model Simulations, Journal of Hydrometeorology, 15, 1091–1116, https://doi.org/10.1175/jhm-d-13-0118.1, https://doi.org/10.1175/jhm-d-13-0118.1, 2014.

Sellers, P., Randall, D., Collatz, G., Berry, J., Field, C., Dazlich, D., Zhang, C., Collelo, G., and Bounoua, L.: A Revised Land Surface Parameterization (SiB2) for Atmospheric Gcms. Part I: Model Formulation, Journal of Climate, 9, 676–705, https://doi.org/10.1175/1520-0442(1996)009<0676:ARLSPF>2.0.CO;2, https://doi.org/10.1175/1520-0442(1996)009$<$0676:ARLSPF>2.0.CO;2, 1996.

Sellers, P. J., Mintz, Y., Sud, Y. C., and Dalcher, A.: A Simple Biosphere Model (SIB) for Use Within General Circulation Models, Journal of the Atmospheric Sciences, 43, 505–531, https://doi.org/10.1175/1520-0469(1986)043<0505:ASBMFU>2.0.CO;2, https://doi.org/10.1175/1520-0469(1986)043$<$0505:ASBMFU>2.0.CO;2, 1986.

Szeto, K. K., Tran, H., MacKay, M. D., Crawford, R., and Stewart, R. E.: The Mags Water and Energy Budget Study, Journal of Hydrometeorology, 9, 96–115, https://doi.org/10.1175/2007jhm810.1, https://doi.org/10.1175/2007jhm810.1, 2008.

Takacs, L. L., Suárez, M. J., and Todling, R.: Maintaining Atmospheric Mass and Water Balance in Reanalyses, Quarterly Journal of the Royal Meteorological Society, 142, 1565–1573, https://doi.org/10.1002/qj.2763, https://doi.org/10.1002/qj.2763, 2016.

Thompson, G., Field, P. R., Rasmussen, R. M., and Hall, W. D.: Explicit Forecasts of Winter Precipitation Using an Improved Bulk Microphysics Scheme. Part Ii: Implementation of a New Snow Parameterization, Monthly Weather Review, 136, 5095–5115, https://doi.org/10.1175/2008mwr2387.1, https://doi.org/10.1175/2008mwr2387.1, 2008.

Trenberth, K. E., Fasullo, J. T., and Mackaro, J.: Atmospheric Moisture Transports From Ocean To Land and Global Energy Flows in Reanalyses, Journal of Climate, 24, 4907–4924, https://doi.org/10.1175/2011JCLI4171.1, https://doi.org/10.1175/2011JCLI4171.1, 2011.

Viterbo, P. and Beljaars, A. C.: An Improved Land Surface Parameterization Scheme in the Ecmwf Model and Its Validation, Journal of Climate, 8, 2716–2748, 1995.

Viterbo, P., Beljaars, A., Mahfouf, J.-F., and Teixeira, J.: The Representation of Soil Moisture Freezing and Its Impact on the Stable Boundary Layer, Quarterly Journal of the Royal Meteorological Society, 125, 2401–2426, https://doi.org/10.1002/qj.49712555904, https://doi.org/10.1002/qj.49712555904, 1999.

West, G. L., Steenburgh, W. J., and Cheng, W. Y. Y.: Spurious Grid-Scale Precipitation in the North American Regional Reanalysis, Monthly Weather Review, 135, 2168–2184, https://doi.org/10.1175/mwr3375.1, https://doi.org/10.1175/mwr3375.1, 2007.

Winton, M.: Amplified Arctic Climate Change: What Does Surface Albedo Feedback Have To Do With It?, Geophysical Research Letters, 33, https://doi.org/10.1029/2005gl025244, https://doi.org/10.1029/2005gl025244, 2006.

Woo, M.-k., ed.: Cold Region Atmospheric and Hydrologic Studies. the Mackenzie Gewex Experience, Springer Berlin Heidelberg, https://doi.org/10.1007/978-3-540-75136-6, https://doi.org/10.1007/978-3-540-75136-6, 2008.

Yang, D., Shi, X., and Marsh, P.: Variability and Extreme of Mackenzie River Daily Discharge During 1973-2011, Quaternary International, 380-381, 159 – 168, https://doi.org/https://doi.org/10.1016/j.quaint.2014.09.023, https://doi.org/https://doi.org/10.1016/j.quaint.2014.09.023, larger Asian Rivers 8: Impacts from human activities and climate change, 2015.

Data availability. The WRF western Canada simulation is available by contacting zhenhua.li@usask.ca. The Era-Interim Reanalysis is accessed through ECMWF's website https://apps.ecmwf.int/datasets/data/interim-full-daily/. The JRA-55 is available at the Research Data Archive of National Center for Atmospheric Research's http://rda.ucar.edu/datasets/ds628.1/. NARR is provided by the NOAA/OAR/ESRL PSD, Boulder, Colorado, USA, from their web site at https://www.esrl.noaa.gov/psd/data/gridded/data.narr.html

Author contributions. TEXT

Competing interests. TEXT

35 *Disclaimer.* TEXT